Remote Sensing of Environment 184 (2016) 506–521

Contents lists available at ScienceDirect

Remote Sensing of Environment

journal homepage: www.elsevier.com/locate/rse

A MODIS-based burned area assessment for Russian croplands: Mapping requirements and challenges

Joanne V. Hall [a,*], Tatiana V. Loboda [a], Louis Giglio [a], Gregory W. McCarty [b]

[a] University of Maryland, Department of Geographical Sciences, 2181 Samuel J. LeFrak Hall, 7251 Preinkert Drive, College Park, MD 20742, USA
[b] United States Department of Agriculture, Beltsville Agricultural Research Service, 10300 Baltimore Ave #302, Beltsville, MD 20705, USA

ARTICLE INFO

Article history:
Received 24 October 2015
Received in revised form 14 June 2016
Accepted 16 July 2016
Available online 4 August 2016

Keywords:
Burned area
Cropland residue burning
Russian Federation
Remote sensing
MODIS

ABSTRACT

Although agricultural burning is banned in Russia, it is still a widespread practice. Accurately monitoring cropland burned area is an important task as these estimates are used in the calculation of cropland burning emissions, which are ultimately utilized in policy making decisions. In this paper we developed an independent estimate of cropland burning in Russia through assessing the capabilities of global burned area products (MCD45A1; Roy et al., 2008 and MCD64A1; Giglio et al., 2009) and our own custom Moderate Resolution Imaging Spectroradiometer (MODIS) based Cropland Regional Area Burned (CRAB) product. An archive of cropland field state samples was generated from very high resolution (<5 m) imagery allowing us a unique perspective into the challenges of mapping cropland burned area through detailed analysis of the Russian agricultural practices. Our analysis showed all three burned area products were unable to map approximately 95% of burn validation samples, demonstrating that the current coarse resolution (defined here as ≥500 m) satellite capabilities are not adequate for accurately mapping burned area associated with agricultural fires. The transient nature of cropland burns and the climatological conditions of the region require multiple subsequent daily overpasses; however, the small spatial scale of the burns requires moderate (defined here as 10–50 m) spatial resolutions. Future opportunities to accurately map cropland burned area may arise with the Sentinel-2 and Landsat constellation missions.

1. Introduction

Anthropogenic transformations of the terrestrial biosphere have greatly altered the earth's land surface. By 2011, approximately 40% of the ice-free land surface had been modified for agricultural activities (FAOSTAT, 2015a). These managed areas have replaced forests, natural grasslands and savannas and have led to a range of impacts on the planet's ecosystem structures and functions (Ramankutty et al., 2008). The impacts of these activities vary greatly due to the differing management practices applied throughout the various global agricultural regions. The use of fire in agricultural management for removal of excess residue and the control of diseases and pests is a common practice across different regions from developing to developed countries (EPA, 2012; McCarty et al., 2012). Although prescribed burning is a useful agricultural management tool, concern is growing in the scientific community regarding the negative consequences on regional climates and air quality due to associated emissions of gases and particulates (Foley et al., 2005).

Impacts from agricultural activities are not limited to areas within these managed ecosystems. Chemical studies of particles deposited on Arctic snow indicate that northern mid-latitude agricultural burning and forest fires are the dominant sources of black carbon (BC) deposition above the Arctic Circle (Hegg et al., 2009; Koch and Hansen, 2005; Pettus, 2009; Stohl et al., 2006). BC is a product of incomplete combustion of carbonaceous fuels and new estimates place BC as the second most important human emission in regards to climate forcing, behind carbon dioxide ($+1.82$ Wm^{-2}; Stocker et al., 2013) with a total climate forcing of $+1.1$ Wm^{-2} with 90% uncertainty bounds of $+0.12$ to $+2.1$ Wm^{-2} (Bond et al., 2013). Unlike the mid- and low latitudes, the Arctic has a unique role in the earth climate system through increased surface reflectance created by the region's high snow and ice albedo. Both natural and human-induced changes to the region's albedo have resulted in the accelerated warming of the Arctic. Specifically the deposition of BC, transported from northern mid-latitudes, is a significant contributor to observed short term warming trends in the Arctic (Bond et al., 2013; Hansen and Nazarenko, 2004; Jacobson et al., 2007; Ramanathan and Carmichael, 2008; Quinn et al., 2008, 2011).

The identification of BC emissions from fires as a contributor to Arctic warming has led to a surge of interest in limiting or eliminating prescribed burning, particularly in spring, to reduce the warming effect of BC (Zender, 2007). There are large uncertainties in the current estimates of the sources, source regions, and transport and transformation pathways of BC transported to the Arctic region (Hegg et al., 2009; Shindell

* Corresponding author.
E-mail address: jhall1@umd.edu (J.V. Hall).

http://dx.doi.org/10.1016/j.rse.2016.07.022

et al., 2008; Quinn et al., 2008) and many of these uncertainties stem from the current inaccurate estimates of cropland burned area. In this paper, we aim to develop an independent estimate of cropland burning in Russia through assessing the capabilities of global burned area products and our own custom Moderate Resolution Imaging Spectroradiometer (MODIS) based burned area product to quantify cropland burning in Russia. Russian agriculture is of global importance, however, relatively little is known about the crop management strategies and in particular the burning practices in rural areas (Pettus, 2009). Russia is the world's fifth-largest wheat exporter and impacts on the wheat harvest can have large implications on global markets (FAOSTAT, 2015b; Grumm, 2011; Kramer, 2010). Although federal law banned open burning, Russia and Kazakhstan are responsible for the largest portions of BC emissions from biomass burning that reach the Arctic, followed by China, the United States and Canada (Pettus, 2009).

Accurate monitoring of the temporal dynamics of prescribed burning is crucial as studies have found that the timing of the burning plays an important role in determining the magnitude of the BC impact on the Arctic (Stohl, 2006; Warneke et al., 2010). In particular, early springtime cropland burning has a surprisingly large impact on the Arctic considering cropland fire injection heights are lower than forest fires and they have a much shorter duration of burning. Even with low injection heights, under the right atmospheric conditions, BC particles can be transported long distances. One such method of low-level transport is related to surfaces of constant potential temperature (Stohl et al., 2007). During the spring, Arctic temperatures are higher, thus reducing the temperature contrast between the northern mid-latitude source regions (40°N and above) and the Arctic (Law and Stohl, 2007). This reduction in the temperature contrast leads to the creation of efficient pollution pathways that facilitate low-level transport of BC from northern mid-latitudes to beyond the Arctic Circle; hence it is imperative to understand both the spatial and temporal patterns of cropland residue burning in the northern mid-latitudes.

Currently, accurate monitoring of cropland burning from existing active fire and burned area products is limited. The transient nature and non-contiguous patches of cropland fires requires a tailored mapping algorithm that is designed to capture the subtle nuances of the cropland spectral signature. Many existing burned area algorithms are focused on mapping hotter and larger wildfire events and several have global extents (MCD45A1; Roy et al., 2008 and MCD64A1; Giglio et al., 2009). Even with regional burned area algorithms (Loboda et al., 2007; McCarty et al., 2008), the inclusion of the MODIS Active Fire Product (MCD14ML; Giglio et al., 2003) as a driver of the mapping algorithm will inhibit the ability to capture the full extent of burning in the cropland regions. For example, McCarty et al. (2008) found that MODIS active fire detections contributed to <4% of the total burned area estimated in the United States croplands within MODIS tile h10v05, which encompasses a large portion of the Mississippi River Delta and the southern Great Plains. In addition, burned area algorithms which do not address small fires, defined as fires smaller than the spatial resolution of the surface reflectance imagery, potentially underestimate the total burned area particularly in cropland regions where fires are both small and transient (McCarty et al., 2009; Randerson et al., 2012; Wu et al., 2015). Recent studies have found that utilizing the MODIS Active Fire product helped identify crop residue burning, particularly in small fields which are not able to be detected through traditional difference Normalized Burn Ratio (dNBR) threshold methodologies (McCarty et al., 2009; Randerson et al., 2012).

In this paper, we focus on the creation of a customized MODIS-based burned area product for the Russian cropland area and the comparison with the existing MCD45A1, MCD64A1 and MCD14ML products to highlight the challenges in mapping cropland burning. Section 2 focuses on the data and methods with particular emphasis on the development of a unique archive of samples extracted from multispectral very high resolution (VHR, defined as <5 m resolution) imagery (Section 2.1) and the development of a customized MODIS-based burned area product (Section 2.2), including the creation of a multi-sensor clear-surface compositing algorithm (Section 2.3). Section 3 focuses on the accuracy assessment, results and intercomparison between the burned area products, followed by a discussion of the challenges of mapping cropland burned area (Section 4) and concluding with recommendations for future cropland burned area studies.

2. Data and methods

The Cropland Regional Area Burned (CRAB) algorithm was designed to improve quantification of the spatial and temporal variability of burned area from Russian cropland residue burning between 2003

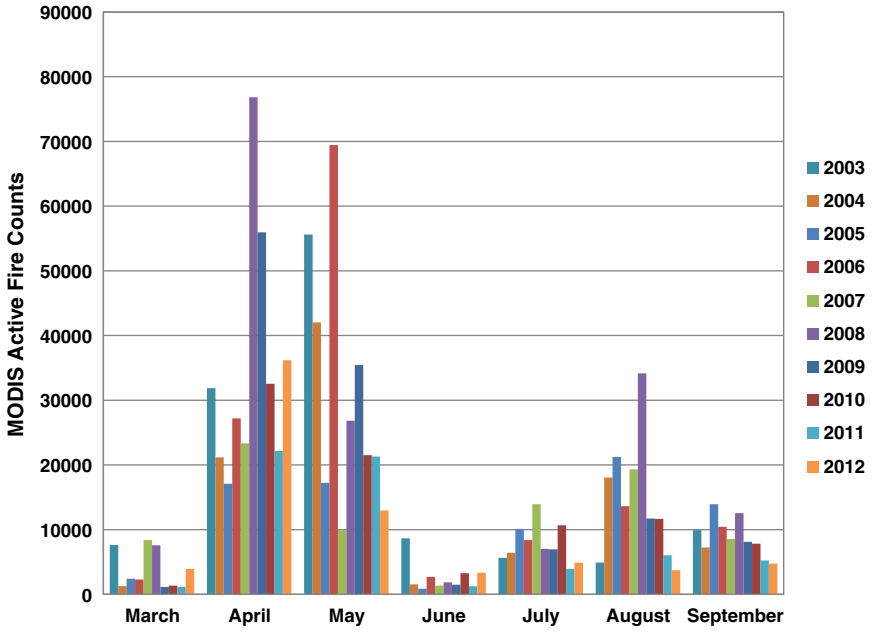

Fig. 1. MODIS Active Fire (MCD14ML; Giglio et al., 2003) counts within the Russian cropland area as defined by the crop mask (see Fig. 4) between 2003 and 2012.

and 2012. The CRAB algorithm maps daily burned area over the Russian cropland at 500 m resolution. The generated outputs include seasonal burned area maps, containing the Julian Date for the mapped burn date for each burn pixel, and confidence layers. The CRAB algorithm is divided into two seasons based on the assumption that croplands can burn more than once a year (e.g. before planting and/or after harvest) thus resulting in two distinct burning seasons: spring (1 March–30 June) and summer (1 July–30 September). These were defined based on the analysis of the frequency distribution of the MODIS Active Fire product (MCD14ML) (Fig. 1) and the general planting and harvesting practices (described below, USDA FAS, 2013). It is further assumed that a given pixel can burn only once during one of the burning seasons (cumulatively no more than twice during a year).

Analysis of the MODIS Active Fire product between March and September 2003 to 2012 revealed an interannual range of approximately 60,000–166,000 active fire counts within the Russian cropland region. The MODIS instrument acquires daily observations of fire activity from two satellites – Terra, launched in late 1999, and Aqua, launched in 2002. Only active fire detections acquired between 2003 and 2012 were included in the analysis to ensure the temporal consistency of the dataset. The variation in the distribution is related to the agricultural practices of the different regions. In particular, a common pattern relates to the spring and winter wheat cycles. Typically the winter wheat campaign begins in mid-August in the Volga District and advances southward. The crops enter dormancy in late October/early November, whereby in an average year, approximately 13% of winter grains are lost over the course of winter due to severe frost damage and other winter weather-related impacts (USDA FAS, 2013). Harvesting of the remaining winter wheat crops begins in late June and concludes in late August. On the other hand, the spring wheat campaign begins in April and the harvest commences in August and is finished by late October. Analysis of the active fire burning distribution, within the Russian cropland region, found that there were generally two distinct burning seasons (Fig. 1), thus the CRAB algorithm was divided into spring (1 March–30 June) and summer (1 July–30 September).

Fig. 2 shows the overall framework of CRAB. Multispectral VHR imagery was acquired from DigitalGlobe's high resolution commercial satellites, QuickBird and World View-2 for the creation of the training and validation samples. The algorithm ingests the daily surface reflectance 500 m Level 2G MODIS imagery acquired from Terra and Aqua (MOD/MYD09GA; Vermote et al., 2011) satellites between 2003 and 2012. A combination of the 1 km quality assessment layers and angle geometry layers were extracted from the Aqua (MYD09GA) and Terra (MOD09GA) datasets and were composited using a multivariate decision making approach to select the best quality observations with intent to minimize false detections (see Section 2.2 for more detail). To ensure the algorithm only processed observations over the Russian cropland region, a crop mask was created using the cropland and cropland/

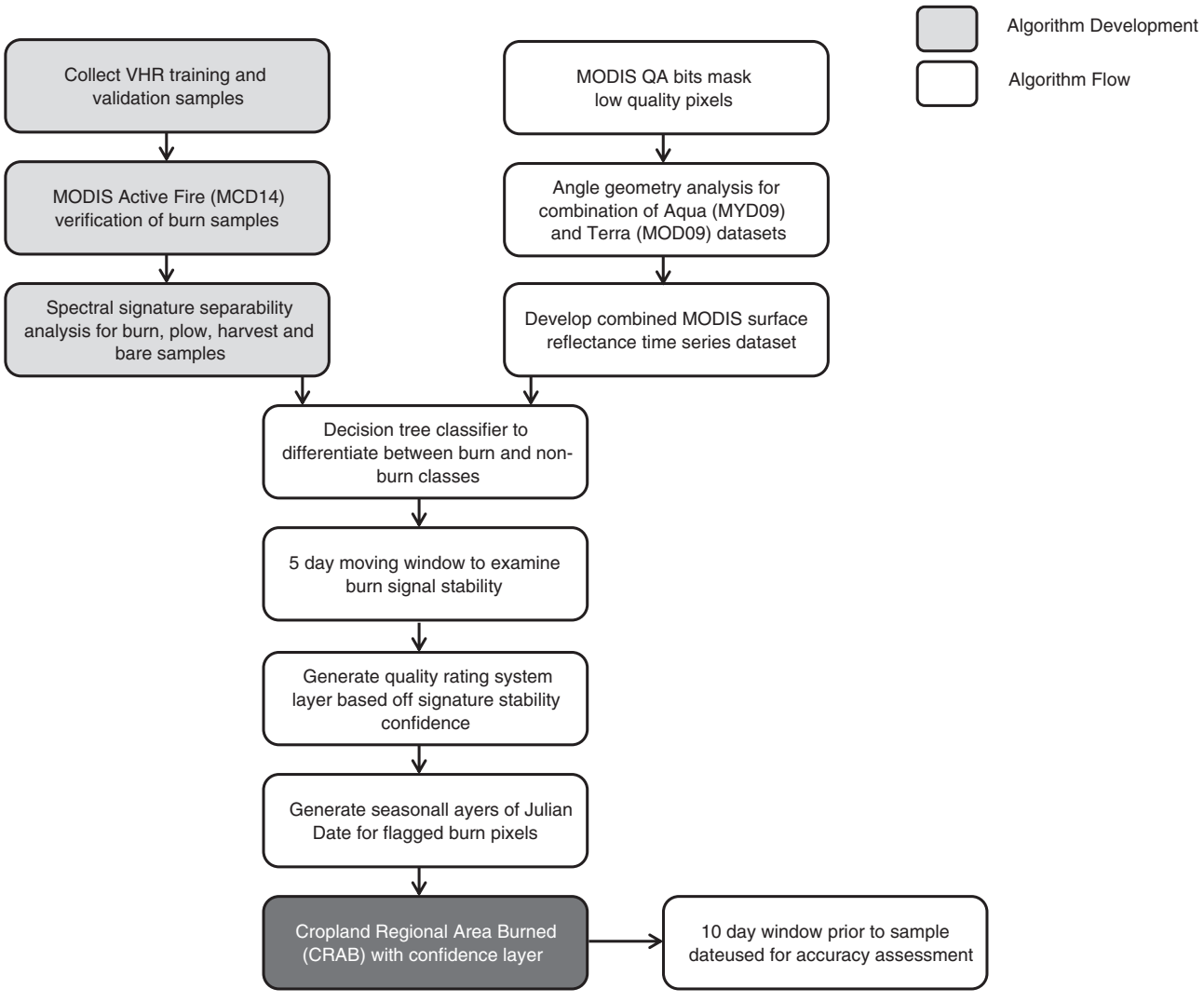

Fig. 2. Cropland Regional Area Burned pre-algorithm development and methodological framework.

natural vegetation mosaic layers from the 2011 500 m Level 3 International Geosphere-Biosphere Programme (IGBP) classification scheme within the MODIS land cover dataset (MCD12Q1; Friedl et al., 2010). After analyzing the variability in the IGBP cropland and cropland/natural vegetation layers, we are satisfied with utilizing this product in the CRAB algorithm (see Supplementary material for more details). In addition, the MODIS 250 m land-water mask (MOD44W; Carroll et al., 2009) was aggregated to 500 m using a strict aggregation rule to avoid water contamination and applied to the IGBP crop mask. The 500 m grid cell was flagged as water if any of the four 250 m grid cells were identified as water. Since wet soil can often trigger a response in the SWIR bands we opted to reduce any confusion with small water bodies.

2.1. Visual assessment of fire practice in Russian croplands from VHR imagery

The high spatial resolution (<5 m) of the multispectral VHR imagery is a much needed element for the identification and discrimination of various cropland field states, including, active fire verified burn, visually identified burn, plow, residue and bare fields (Fig. 3). A particular challenge with cropland burned area mapping is the difficulty in distinguishing burned from plowed fields (McCarty et al., 2009; Roy et al., 2005). The VHR imagery allows for more accurate identification of field condition through visual interpretation and from the incorporation of the MODIS Active Fire (MCD14ML) dataset as a means of independent validation for the selection of burned training and validation samples (see Section 2.1.3).

For our archive, dark, smooth textured fields were digitized as plowed. Typically these fields were fairly homogenous and the dark uniform color filled the entire field area (Fig. 3c and e), whereas burns without the flaming front were identified by the rough texture and natural fingerlike patterns created from the moving flaming front (Fig. 3f).

Quantifying the extent and magnitude of cropland burning is a challenging task as there is little consensus amongst the available data. Visual analysis of the VHR imagery reveals a larger proportion of cropland burned area than what is indirectly detected through the MODIS Active Fire product and what has been reported by farmers through telephone surveys undertaken as part of a USDA Black Carbon Initiative project (SovEcon, 2013). According to the survey results, farmers have noticed a significant reduction in agricultural burning, with some respondents claiming agricultural burning has not been observed in the Rostov region for at least the last 10 years, the Stavropol region for 5–7 years, the Krasnodar region for 2–5 years, the Saratov region for 3 years, and the Altai region for 2 years (Fig. S1). However, the survey results also claim that mainly small agricultural enterprises in these regions still burn for a variety of reasons which include the reduction of soil harbored plant diseases in the Rostov region and the removal of straw for the improved crop planting and germination success in areas of the Saratov and Voronezh regions. Further analysis of the active fire product revealed burning in all these areas between 2003 and 2012; however, the magnitude and temporal distribution varied across all regions.

2.1.1. Archive development of field samples under various post-harvest conditions (burn, bare, standing crop residue, plowed) from VHR imagery

We have created an archive of various field state samples within the Russian cropland region from VHR imagery (Fig. 4). The VHR samples were visually identified and digitized by several image analysts (for

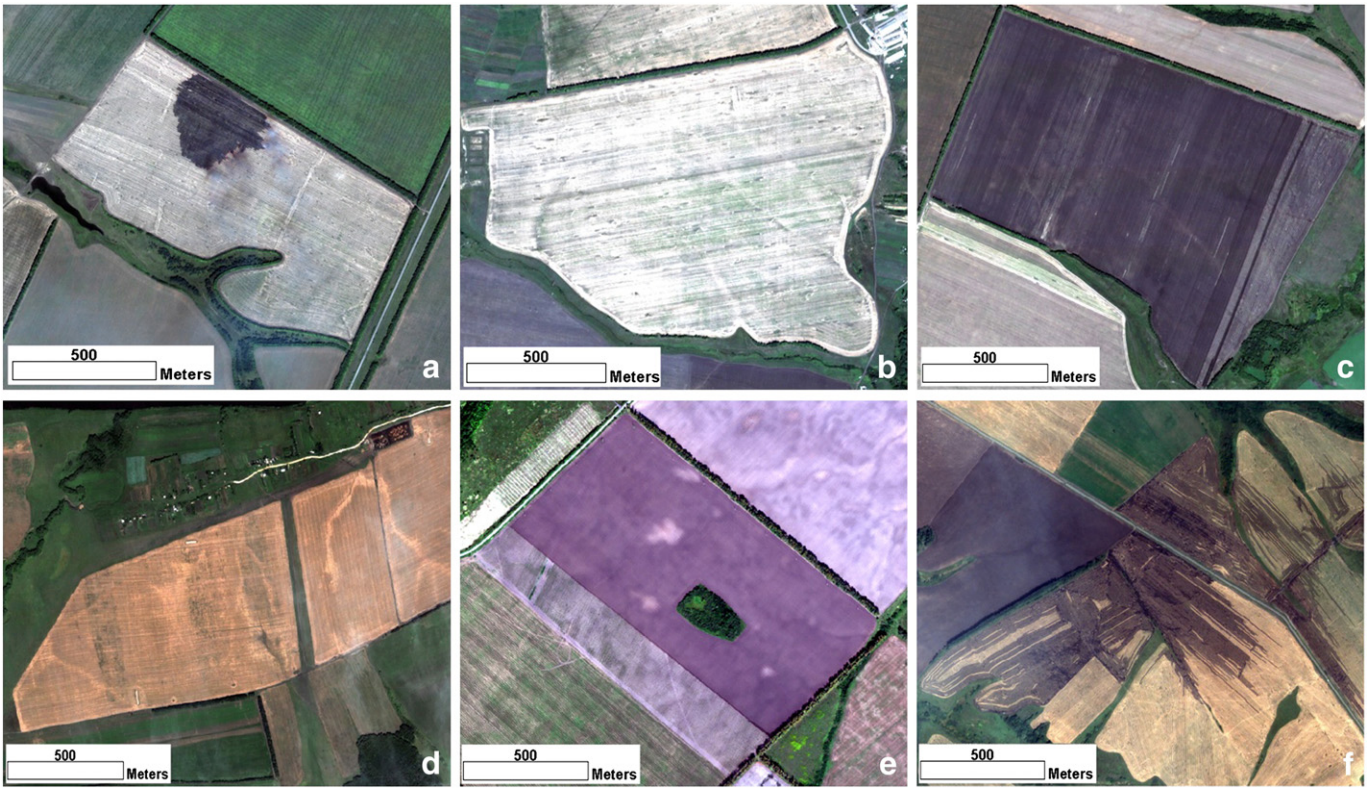

Fig. 3. Very high resolution (<5 m) field state examples: burned field (a and f), residue field (b), freshly plowed field (c and e) and bare field (d). Fig. 3a shows a burn with a flaming, smoking front which is easily identifiable as a burned field, whereas burned fields without flaming fronts (Fig. 3f) are identified by the natural fingerlike patterns created from a moving flaming front. Typically these burned area examples are located within residue fields. Fig. 3b identifies a residue field which is a brighter field, typically with linear features which correspond to the rows of residue stubble. Plowed fields (Figs. 3c and e) are identified by a dark, smooth texture which tends to start at the field edges. Bare fields (Fig. 3d) are fields which do not contain large amounts of residue or vegetation and do not show any signs of a fresh burn or plow. Images are displayed using the true color composite.

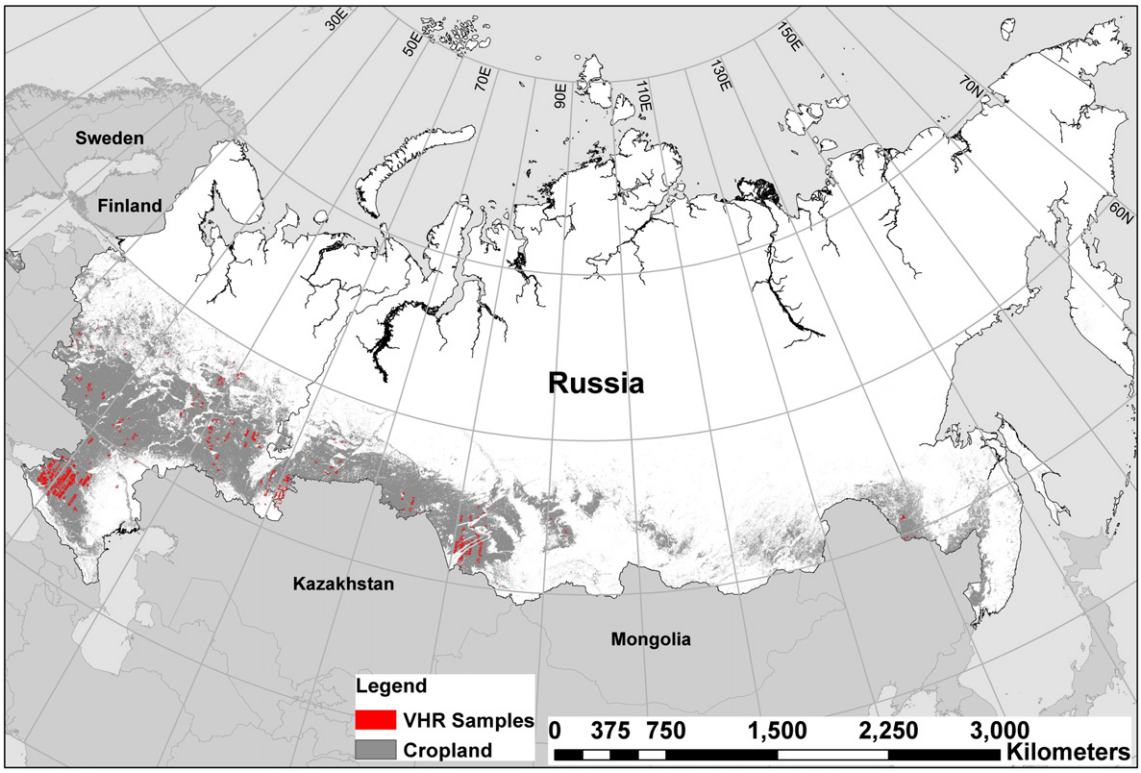

Fig. 4. Very high resolution (<5 m) samples (2003 – 2012) acquired from DigitalGlobe's high resolution commercial satellites, QuickBird and World View-2 overlaid over the Russian cropland.

details see Section 2.1.3). The low repeat frequency of VHR satellites and their small footprint size (e.g., ~360 km × 18 km for QuickBird) leads to an opportunistic acquisition strategy and therefore the archive does not cover the full extent of the Russian cropland region.

From the analysis of the active fire counts, it is clear there is a substantial amount of burning within Russian cropland. Using the archive of VHR data, we examined these burns in greater detail than can be accomplished through the current MODIS products. This archive allows us a unique perspective into the challenges of mapping cropland burned area through the detailed analysis of the Russian agricultural practices. Table 1 below presents the size distribution of the entire VHR sample archive. Analysis of the size distribution of the cropland burns and field samples found a large proportion of the burn and non-burn samples occupying <21 ha, which is the approximate equivalent of one 463 m MODIS grid cell.

Depending on the exact configuration of the field relative to the 500 m MODIS sinusoidal grid, the actual relationship between the MODIS grid cells and the sizes of burned or total field areas can be substantially smaller. Here we are presenting the best case estimates. Furthermore, in general the burned area samples are smaller than the field area as only the burned portion of the field was digitized when creating the burn sample. The distribution of field sizes and burned area both have a positively skewed relationship (Fig. 5) with the majority of burns occupying <50 ha.

Table 1
Distribution of burn and non-burn samples digitized from very high resolution (<5 m) imagery. Values in parentheses are approximate equivalent MODIS 500 m grid cells based on the size of the samples in hectares.

	Burn Samples	Field Samples
Minimum, ha (~grid cell)	0.5 (<1)	2.4 (<1)
Maximum, ha (~grid cell)	411 (20)	656 (31)
Mean, ha (~grid cell)	57 (3)	88 (4)
Median, ha (~grid cell)	40 (2)	71 (3)
Standard Deviation, ha (~grid cell)	56 (3)	68 (3)
Skewness	2.3	1.9
Kurtosis	7.8	5.6
Total Number of Samples	782	6037

2.1.2. Visual examination of burn strategies identified in VHR imagery

Further analysis was carried out on the burn samples to identify any additional potential challenges. Visual examination of burning practices in the available VHR imagery found a variety of burning strategies including, complete field burns, partial field burns and pile burning (Fig. 6).

From visual analysis, the full burns (Fig. 6a) are associated with burns that leave little to no unburned residue in the burn extent that can be seen in the VHR image, whereas the partial burns (Fig. 6b and c) include varying degrees of unburned residue within the burn extent. Depending on a number of factors including the amount of biomass within the field and local burn conditions, these partial burns can cover the entire field extent (Fig. 6c) or can only begin to burn in a small section of the field (Fig. 6b – blue circle). Finally pile burns (Fig. 6d) are associated with setting fire to piles of residue. Analysis of the VHR burn samples revealed that the practice of pile burning has an impact on the burn spectral signature due to the larger percentage of non-burned residue within the burned area extent. Although excluding both pile and partial burn samples would improve the purity of the burn spectral signature, the majority of the burn samples are not full burns and do not give a good representation of the agricultural burn practices within Russia (as seen in the VHR archive). Furthermore, visual analysis of the VHR archive found additional nuances in the agricultural practices including fields which were not burned before plowing (see Fig. S2). These variations in agricultural practices and the hesitancy of

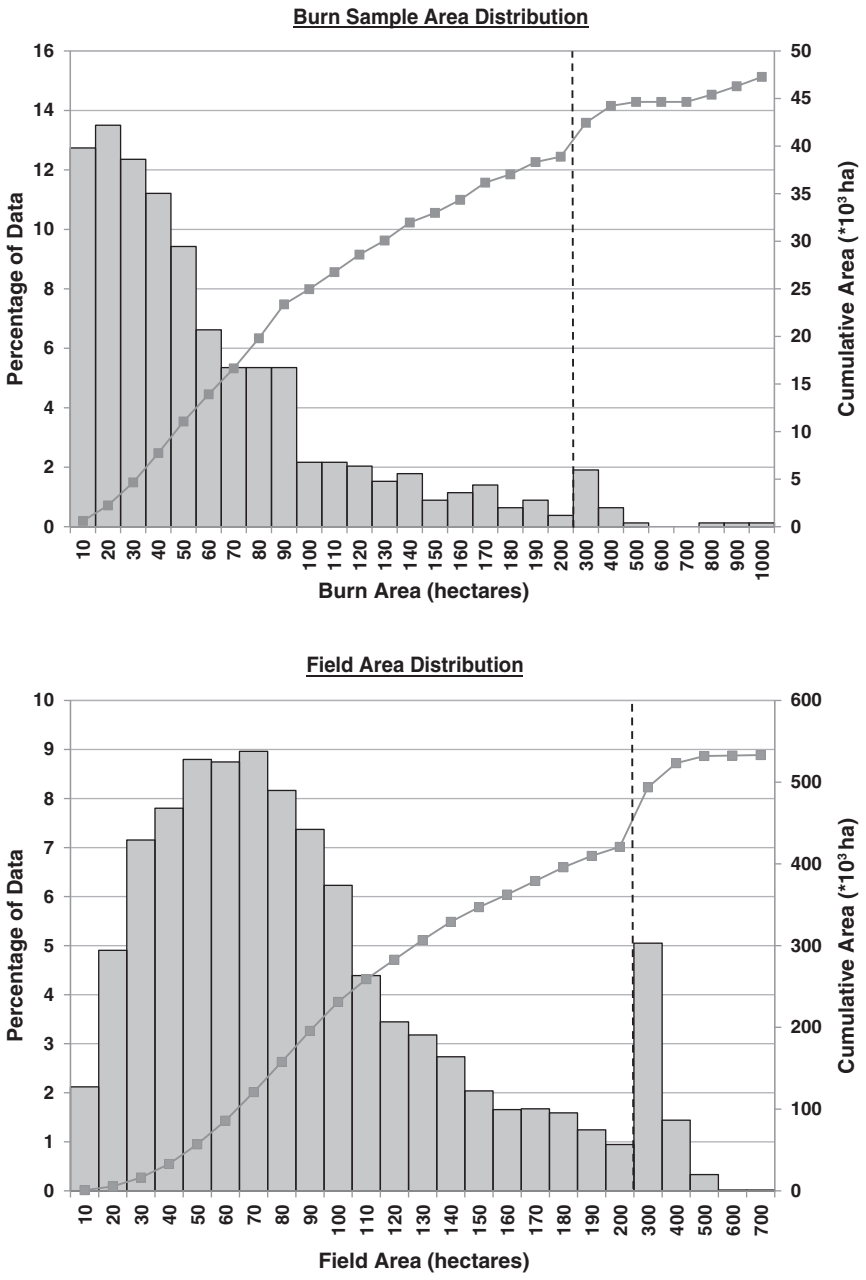

Fig. 5. Burn sample area (above) and field area (below) frequency distributions and cumulative area ($\times 10^3$ ha) for all VHR polygon samples before the matching process. The vertical dashed line indicates a change in area size categories along the horizontal axis.

farmers to disclose their burning methods leads to further hindrances on the ability to accurately map cropland burned area.

2.1.3. Methodology for the development of the post-harvest field condition archive

To assist the image analysts in the initial sorting of the VHR images, the MODIS Active Fire product was incorporated to highlight any VHR images with a potential active fire within ten days of the image date. Each VHR image was then examined and any burns within approximately a 1 km radius, to account for off nadir viewing angle geolocation inaccuracies, of the Active Fire point were manually digitized and classified as an active fire verified burn. Any burns which were not highlighted by the Active Fire dataset, but were visually identified by the analyst, were classed as a burn and not an active fire verified burn. Visually identifiable burned fields constituted a very small fraction of all fields in the processed VHR imagery. For each processed image, the analysts were instructed to digitize all burns and collect 5 samples per non-burn field state (plow, bare and residue) whether the image contained any burned fields or not. Following the manual digitization of the VHR imagery by an image analyst and subsequent collection of the various field type samples (burn, plow, bare and residue), the samples were georegistered to orthorectified Landsat imagery and then geometrically matched through the rasterization of the VHR polygons to the 500 m Level 2G MODIS imagery (MOD/MYD09GA; Vermote et al., 2011). Approximately 4% of the burn samples (average size ≤1 MODIS grid cell) were lost during the matching process as the

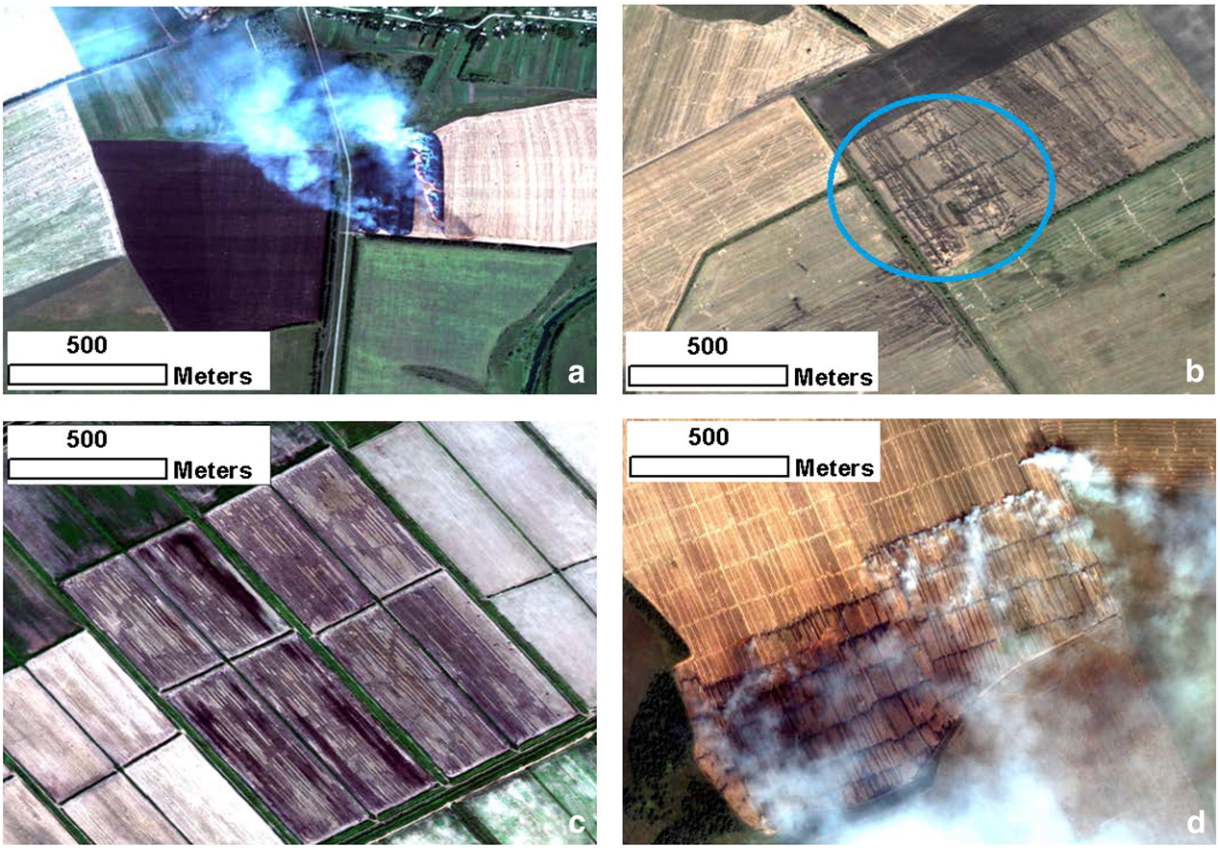

Fig. 6. Visual burning practices found in available very high resolution (<5 m) imagery: complete field burn (a), partial field burn (b), partial field burn (c), and pile burn (d).

configuration of the field sample relative to the 500 m MODIS grid cell led to the splitting of the sample between adjacent grid cells and therefore the smaller samples were unable to be rasterized to the coarser MODIS resolution based on the 50% majority aggregation rule. Upon completion of the matching process, the field samples were temporally stratified by typology based on a randomized sampling scheme to separate the samples into training or validation categories based on the dates and field type. The final totals of VHR spring and summer samples are highlighted in Table 2.

2.2. Clear surface analysis

Accurate mapping of cropland burned area requires multiple subsequent daily observations to alleviate one of the largest sources of error being the inability to distinguish burned from plowed fields. This is particularly relevant in the Mollisol regions of southern Russia (McCarty et al., 2009; Roy et al., 2005). Although MODIS imagery is acquired daily, the time series is not continuous as periods of prolonged clouds, aerosols and snow can limit the number of available clear surface days. A new compositing algorithm has been developed to combine Aqua and Terra data to improve the availability of clear surface views and to avoid forward scattering which results in artificial darkening of the spectral signature. The 1 km MODIS quality assessment (QA) data layers were extracted from the MOD09GA and MYD09GA products for use in the clear surface analysis over the Russian cropland region as defined by the crop mask. Each image contains a corresponding QA layer which holds 16 bit flags that summarize 11 different parameters. For this analysis, only bits related to clouds, aerosols and snow were chosen (Table S1). The QA bits were extracted into daily binary layers, representing the clear surface days for both Aqua and Terra.

Table 2
Very high resolution (<5 m) spring and summer samples matched to MODIS 500 m grid cells.

	Training	
	Spring	**Summer**
Burn	480 grid cells	1312 grid cells
Bare	835 grid cells	3171 grid cells
Residue	693 grid cells	3401 grid cells
Plow	662 grid cells	2491 grid cells
	Validation	
	Spring	**Summer**
Burn	369 grid cells	762 grid cells
Bare	762 grid cells	1872 grid cells
Residue	527 grid cells	1996 grid cells
Plow	579 grid cells	1616 grid cells

2.3. Multi-sensor clear surface composite

Due to the non-Lambertian nature of cropland fields, the bidirectional reflectance characteristics varies considerably, leading to large differences in the observed reflectance (Rahman et al., 1999; Ranson et al., 1985; Schaaf et al., 2002). Analysis from a sample field's spectral output illustrates the impact on the burn spectral signature (Fig. 7). Reflectance values are expected to decrease in the visible and near infrared bands following a burn due to the deposition of char on the brighter soil surface (Zhang et al., 2003). This decrease is visible in Terra's output following the burn on Julian Date 229 (17 August 2006, 10:04:20 MSK; Fig. 7b), whereas there is a clear increase in reflectance in the spectral output of Aqua (17 August 2006, 12:11:09 MSK; Fig. 7c). Further analysis on the solar and view zenith and azimuthal angles found the discrepancies in reflectance values between the two datasets were related to the differing

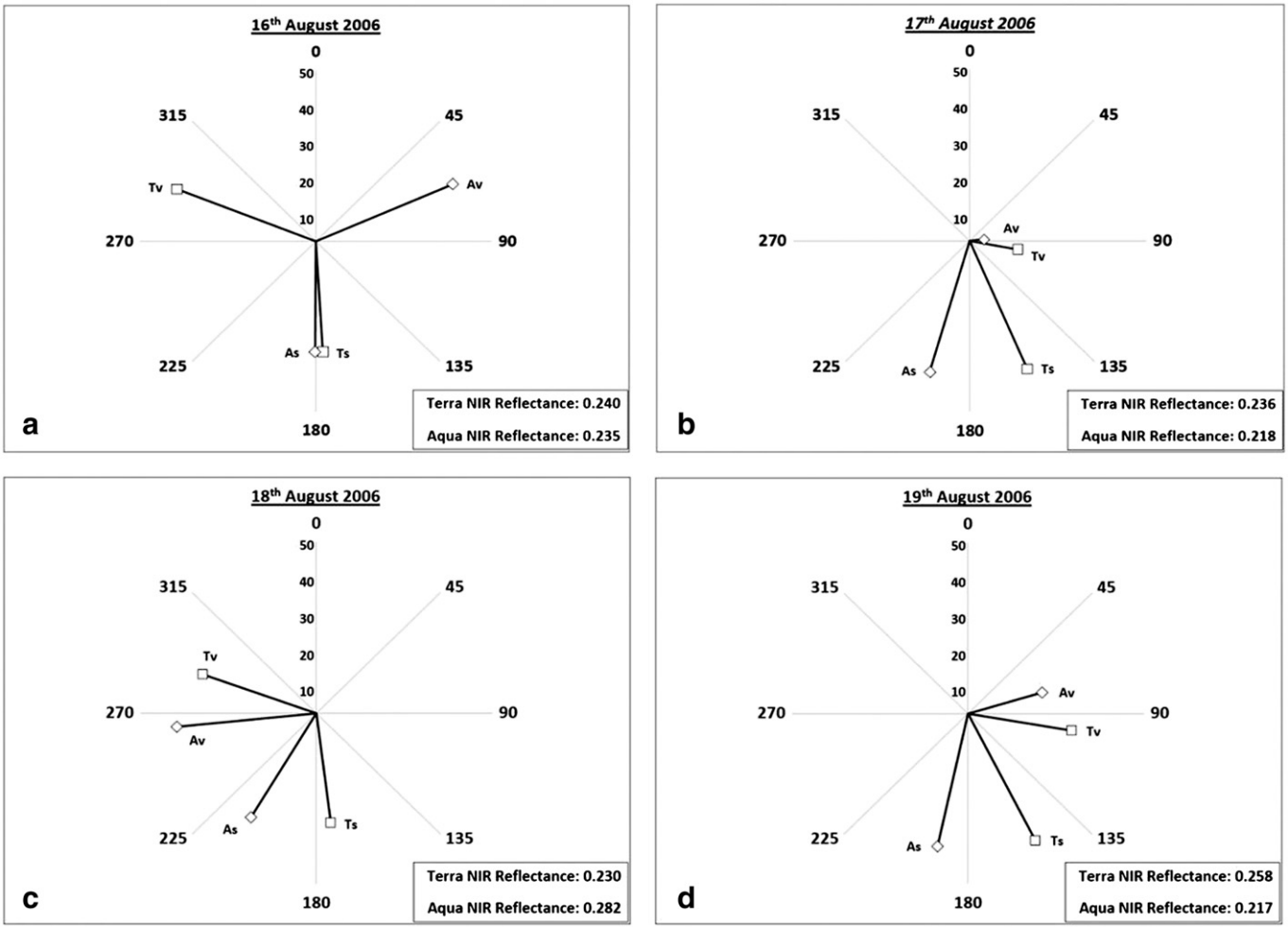

Fig. 7. Solar (Ts, As) and sensor (Tv, Av) azimuthal and zenith angles for Terra and Aqua over 16–19 August 2006. The verified active burn occurred on 17 August 2006. The zenith angles are represented by the radius of the black line. Zenith angles scaled between 0° and 50° for visualization. The near infrared reflectance (NIR) values are located in the lower right boxes.

solar and viewing angle geometries and it is clear that the higher reflectance values correspond to a back scatter scenario with zenith angles far off nadir (Fig. 7c). This same pattern is seen in a number of studies whereby the reflectance values generally decrease from the backward to the forward scattering direction (e.g. Galvao et al., 2009; Rahman et al., 1999).

The following method outlining the combination of Aqua and Terra daily observations aims to minimize the impact of bidirectional reflectance distribution function (BRDF) related decreases in surface reflectance with the general aim to lower the commission error of the CRAB product (Fig. 8).

In the combination of the two datasets, the solar zenith (SZ), view zenith (VZ), solar azimuth (SA) and view azimuth (VA) angles were extracted from the MOD09GA and MYD09GA products. Following the outline in Fig. 8, the angle geometry algorithm ingested the four angles for the creation of the three variables used in the calculation of the Viewing Indicator Geometry (VIG) index:

Variable 1: Linearly scaled solar zenith angle (SZ_s) for both Aqua and Terra between 0 (90° off nadir = undesired) and 1 (nadir = desired).

Variable 2: Linearly scaled absolute azimuthal difference (AD_s) for both Aqua and Terra between 0 (0° or 180° diff = undesired) and 1 (90° diff = desired). We preferred to avoid forward scattering (artificial darkening) and backward scattering (artificial brightening) and rather considered values between both situations.

Variable 3: Linearly scaled view zenith angle (VZ_s) for both Aqua and Terra between 0 (90° off nadir = undesired) and 1 (nadir = desired).

The three variables were summed and weighted equally in the calculation of VIG. The difference between VIG Aqua and VIG Terra (dVIG) was evaluated against our chosen threshold. If the difference was less than −0.15 Aqua was chosen; whereas if the difference was >0.15 then Terra was chosen. If the value lay between these two thresholds then the smallest azimuthal difference, corresponding to a back scatter scenario, as calculated in variable 2 was chosen. The composition process can be seen in Fig. 7. On 16 August 2006, the VIG values are almost identical, leading to a small dVIG (−0.03). According to the threshold criteria, the low dVIG requires the lowest AD_s value to be chosen. In this instance Terra was slightly closer to 90°, whereas on 17 August 2006 Aqua's geometry was preferred as Terra was closer to a more intense backscatter scenario. In this instance Aqua was preferred as Aqua's VZ angle was also closer to nadir. The combination angle geometry and clear surface layers created a combined multi-sensor clear surface composite which was subsequently utilized in the CRAB algorithm (Fig. 2).

2.4. Burned area map and confidence level development

Upon completion of the clear surface composite, a single daily image of clear surface observations combined from Terra and Aqua is evaluated for burned area detection. The CRAB algorithm uses a decision tree

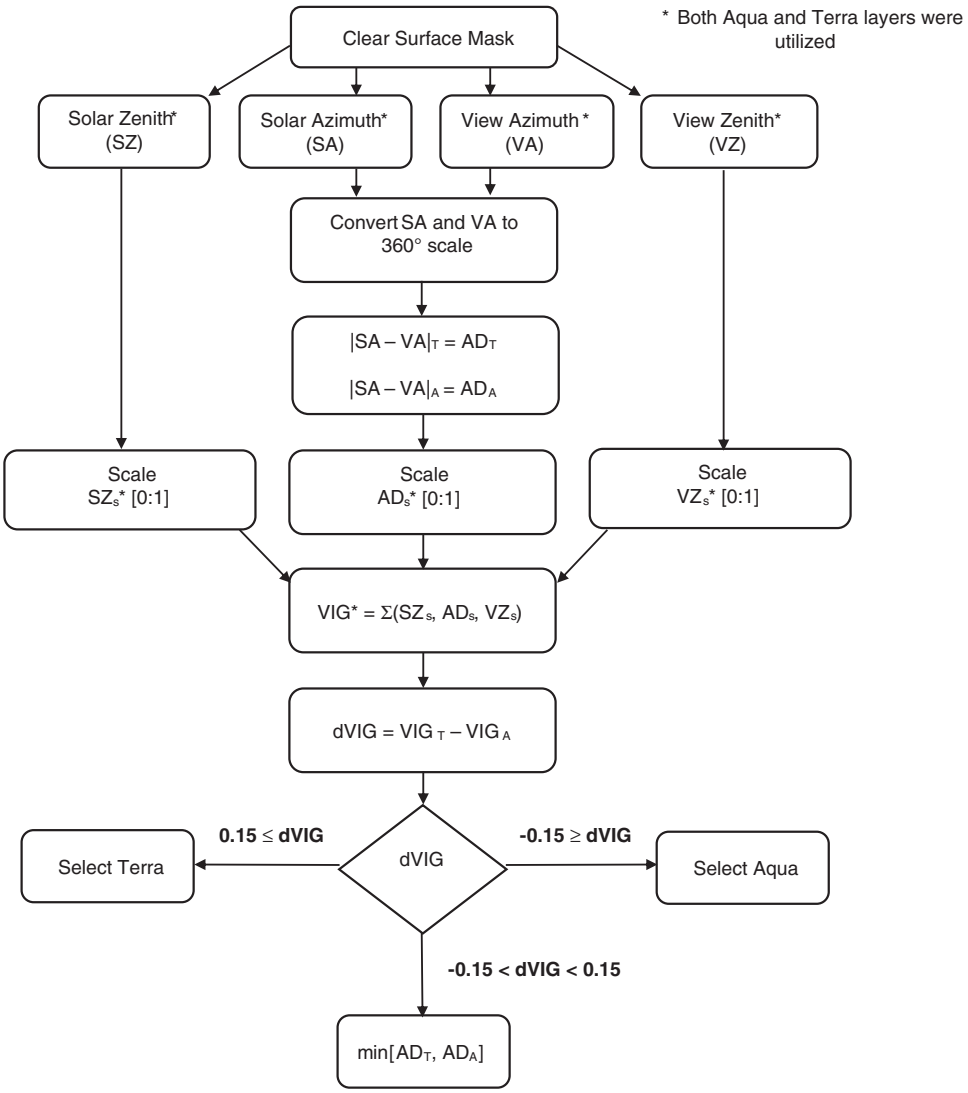

Fig. 8. Methodological framework for the combination of Aqua and Terra clear surface datasets into one BRDF adjusted time series.

classifier that differentiates between burn and non-burn (residue, plow and bare) classes and assigns a probability to each of the burn terminal nodes. A total of 690 training fields (116 burned and 574 unburned) were utilized in the spring classification tree and 2249 training fields (326 burned and 1923 unburned) were utilized in the summer tree. A set of 12 metrics was created as an input into the decision tree for each burn and unburned training sample split between the two mapping seasons, spring and summer. These inputs were a combination of spectral reflectance bands (ρ); band 1 (620–670 nm), band 2 (841–876 nm), band 3 (459–479 nm), band 4 (545–565 nm), band 5 (1230–1250 nm), band 6 (1628–1652 nm) and band 7 (2105–2155 nm), and derived spectral indices, including; Normalized Burn Ratio ($[\rho_2 - \rho_7]/[\rho_2 + \rho_7]$; Lopez and Caselles, 1991), Normalized Difference Vegetation Index ($[\rho_2 - \rho_1]/[\rho_2 + \rho_1]$; Rouse et al., 1974), Vegetation Index ($[\rho_5 - \rho_7]/[\rho_5 + \rho_7]$; Giglio et al., 2009) and Normalized Difference Water Index (Gao, 1996) for both band 5 ($[\rho_2 - \rho_5]/[\rho_2 + \rho_5]$) and band 6 ($[\rho_2 - \rho_6]/[\rho_2 + \rho_6]$).

An output decision tree was generated for each of the two seasons. The spring tree has 29 terminal nodes of which seven classify burned fields and 22 classify unburned fields with an overall misclassification rate of 11%. The summer tree has six terminal nodes of which one classifies burned fields and five classify unburned fields with an overall misclassification rate of 14%. The spring tree utilized all input metrics for the classification of the burned fields while the summer tree only utilized

Table 3
CRAB burned area classification rules (A–G) for spring and (A2) for summer. A field is classified as burned if it satisfies each condition in any of the classification rules.

Rule	Classification rule (AND)
A	ρ_4 (<0.081); NDVI (<0.302); NDWI6 (< −0.230); NBR (> −0.291); NBR (< −0.236); NDWI6 (> −0.302)
B	ρ_4 (<0.081); NDVI (<0.302); NDWI6 (< −0.230); NBR (> −0.291); NBR (< −0.236); NDVI (<0.284); NDWI5 (< −0.131)
C	ρ_4 (<0.081); NDVI (<0.302); NDWI6 (< −0.230); NBR (> −0.291); NBR (< −0.236); NDVI (>0.284)
D	ρ_4 (<0.081); NDVI (>0.302); ρ_1 (<0.034); ρ_5 (<0.291); ρ_3 (>0.016)
E	ρ_4 (<0.081); NDVI (>0.302); ρ_1 (>0.034); NDWI5 (<0.007); NDWI6 (> −0.317); ρ_5 (<0.261); ρ_7 (>0.179); ρ_7 (<0.134)
F	ρ_4 (<0.081); NDVI (>0.302); ρ_1 (>0.034); NDWI5 (<0.007); NDWI6 (> −0.317); ρ_5 (<0.261); ρ_7 (>0.179); ρ_7 (>0.134); ρ_2 (<0.198); ρ_4 (<0.765); NDVI (>0.404); ρ_6 (<0.239); VI (>0.196)
G	ρ_4 (<0.081); NDVI (>0.302); ρ_1 (>0.034); NDWI5 (<0.007); NDWI6 (> −0.317); ρ_5 (<0.261); ρ_7 (>0.179); ρ_7 (>0.134); ρ2 (<0.198); ρ_4 (>0.765)
A2	ρ_6 (<0.325); NDWI5 (> −0.156); ρ_1 (<0.113); ρ_3 (>0.041); NBR (< −0.194)

ρ_1, ρ_3, ρ_6, NBR and NDWI5 in the classification of the burned fields. The classification rules for each season's tree are reported in Table 3.

The algorithm is designed to monitor the spectral signature and look for a persistent burn signal over a five-day moving window. The CRAB product is generated for each season between 2003 and 2012; however, the algorithm is computed on a daily time step. Each seasonal output has a corresponding confidence layer, which was determined through using a five-day weighting scheme (Conf. $= 0.4\ day_1 + 0.2\ day_2 + 0.1\ day_3 + 0.1\ day_4 + 0.1\ day_5$) over five consecutive days to check for signal stability (here day_i represents the original confidence values assigned from the decision tree nodes for the i'th day within the five-day window). The final output records the date of burn detection, which was assigned on the first day that the spectral thresholds were crossed, within the season and the confidence of burning.

The CRAB product is comprised of two separate decision trees because the biophysical conditions are vastly different between spring and summer. The spring burning conditions are extremely challenging as the excess moisture in the soil from the snow melt lowers the surface reflectance across the full visible – SWIR range with a particularly strong impact on the SWIR range resulting in further diminished spectral separability between burned and unburned fields. In contrast, in the summer soils are substantially drier as compared to the post snow melt period in the spring and fields are typically covered in either crop residue or regrowth of weeds, both detectable in the NIR range. However, even in the summer plowed and wet fields can still be easily confused with burns because of the small difference in reflectance across all bands. Due to these differences, we empirically determined that burned grid cells below a confidence of 60% for the CRAB spring product are not as reliable as in the CRAB summer product and therefore we have applied a mapping confidence threshold of >60% for the CRAB spring product in the subsequent analysis. Fig. 9 illustrates an example of the CRAB output for summer 2012 for all confidence values. The grey denotes the cropland region. The inset highlights the grid cell based Julian Date of burn detection.

Upon creation of the CRAB seasonal burned area maps and corresponding confidence layers, the product's accuracy was assessed using the VHR validation samples and compared to the MCD45A1, MCD64A1 and MCD14ML products. All three burned area products (MCD45A1, MCD64A1 and CRAB) are designed to map burned area and are based on differing principles. MCD45A1 is based on the deviation from the anticipated reflectance change due to burning with applied corrections for BRDF. MCD64A1 is based on the dynamic spectral thresholds generated from a burn sensitive vegetation index coupled with the inclusion of the MODIS active fire observations and a measure of the change in temporal texture following a potential burn. CRAB is a decision tree based algorithm constructed from a suite of spectral bands and indices with observations selected to minimize BRDF effects.

3. Results and discussion

3.1. Accuracy assessment

An accuracy assessment was carried out on CRAB using a ten-day window prior to the date of the validation samples. Due to cloud obscuration of the land surface, a ten-day window is required to enhance the probability of mapping the cropland burns. Our decision to use a window of this duration was based on the transient nature of cropland fires and the potential of plowing or reseeding soon after a burn. The persistence of these low biomass burn scars varies as a function of climate, fuel load and crop management practices. Several studies focusing on grass dominated systems such as cropland, savanna and grasslands have found that the persistence of the burn scars is short lived (days

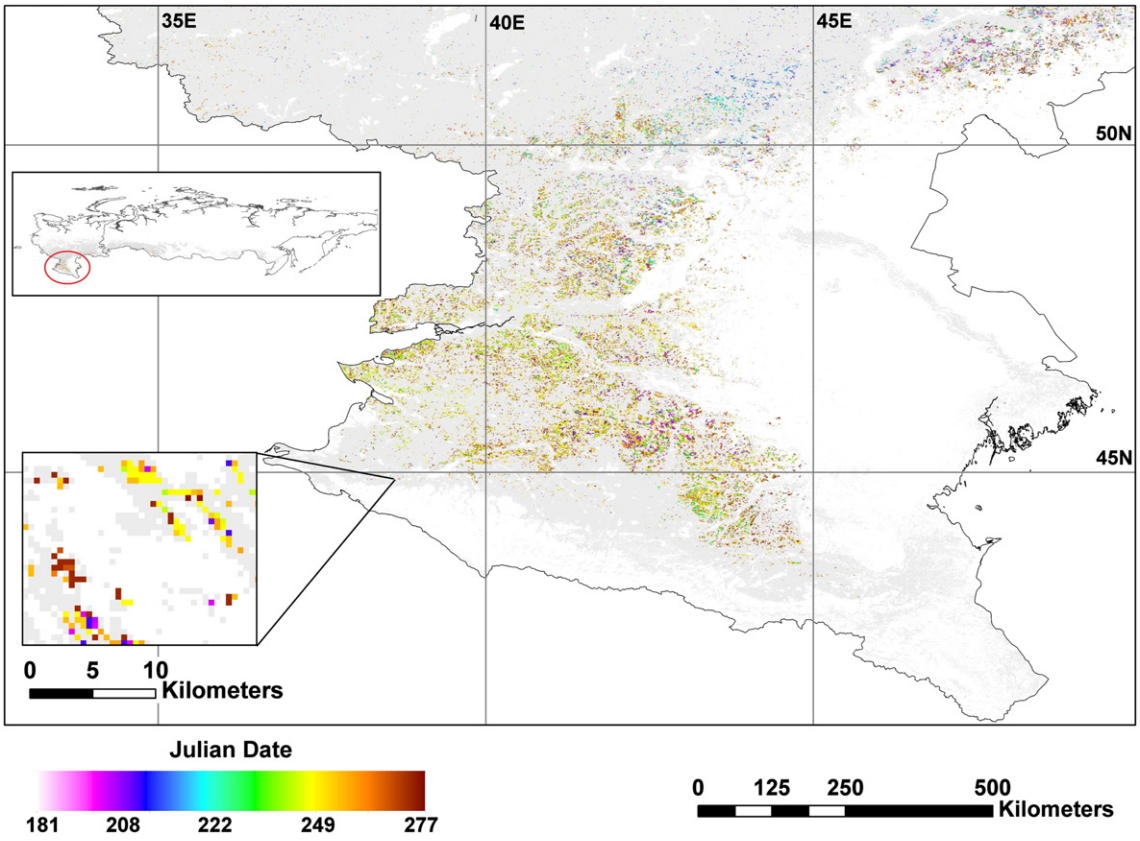

Fig. 9. Summer 2012 CRAB product output. A subset of Russia (red circle, top insert) is shown for display purposes. Colors represent Julian Date of burn. Grey area denotes the Russian crop mask.

Table 4
Spring and summer accuracy assessment comparison between the Cropland Regional Area Burned (CRAB) product and the two official MODIS burned area products MCD45A1 and MCD64A1. The spring assessment was carried out using the full range of CRAB confidence values and >60% confidence. The active fire assessment results (MCD14ML shown in italics) are based on the number (percentage) of intersections by a 1 km radius buffered active fire point within ten days of the image date.

		Commission error			Omission error
		Residue	Bare	Plow	Burn
Spring	**CRAB (all conf.)**	9.11	9.97	10.36	86.98
	CRAB (> 60%)	0.00	0.00	0.00	99.42
	MCD45A1	0.00	0.00	0.86	97.30
	MCD64A1	0.00	0.00	0.00	99.19
	MCD14ML	*0.42*	*0.38*	*1.84*	*91.54*
Summer	**CRAB (all conf.)**	0.45	1.28	4.27	96.86
	MCD45A1	0.60	0.91	2.66	92.65
	MCD64A1	0.00	0.00	0.00	96.73
	MCD14ML	*1.20*	*1.90*	*1.60*	*89.70*

to weeks) and therefore long temporal windows are likely to lead to an increase in burn area omission errors (Korontzi et al., 2008; Trigg and Flasse, 2000). In addition, for regions with double cropping, such as in the Mississippi River Valley, a field can go from harvest to burning and reseeding in a few days to two weeks (Korontzi et al., 2008). This quick turnover and short burn-scar persistence justifies the use of a comparatively short temporal window. While the optimal duration of this value is debatable, it is evident that a 30 day window is too long as the burn signals are virtually always lost to weathering and/or plowing within this period of time (Chuvieco et al., 2008).

Here the samples were applied to the Julian Date of burn detection as described by the CRAB product. If the pixels associated with the validation samples were flagged as burned within a ten-day window prior to the date of the image, then it was counted in the accuracy assessment. An assessment using the VHR spring and summer validation samples was carried out between CRAB, MCD45A1 and MCD64A1 (Table 4). Additionally MCD14ML was assessed to identify the number of VHR validation samples that were intersected by a 1 km radius buffered active fire point within ten days of the image date.

All four products (MCD45A1, MCD64A1, MCD14ML and CRAB) were unable to map approximately 95% of the burn validation samples during summer (93%, 97%, 90% and 97% omission errors, respectively), while in spring there was an improvement using the CRAB product with full confidence values (97%, 99%, 92% and 87% omission error, respectively); however, applying a confidence of >60% led to a CRAB omission error of 99%. The reduced commission error in the MCD45A1 and MCD64A1 products as compared to the CRAB product are due in part to the restrictiveness of their algorithm's spectral mapping thresholds. The mapping thresholds for CRAB can be constrained further to reduce commission error; however, this causes an increase in omission error.

Table 5
Spring cropland burned area (units: $\times 10^4$ km^2 = Mha) comparison between CRAB, MCD45A1 and MCD64A1.

	Spring: Total burned area in Russian croplands			
	CRAB (all conf.)	CRAB (>60%)	MCD45A1	MCD64A1
2003	126	1.91	6.87	4.78
2004	133	2.70	2.74	0.98
2005	121	1.36	1.41	0.49
2006	128	3.19	4.90	1.45
2007	118	2.70	3.09	1.05
2008	135	2.31	7.79	6.18
2009	139	2.17	5.74	3.00
2010	138	1.86	2.32	0.64
2011	132	2.20	3.27	1.12
2012	131	1.40	3.66	1.32

Table 6
Summer cropland burned area (units: $\times 10^4$ km^2 = Mha) comparison between CRAB, MCD45A1 and MCD64A1.

	Summer: Total burned area in Russian croplands			
	CRAB (all conf.)	CRAB (>60%)	MCD45A1	MCD64A1
2003	1.63	0.00075	2.04	0.54
2004	2.34	0.0022	2.12	1.08
2005	3.43	0.0014	3.61	1.64
2006	3.38	0.0041	3.40	1.35
2007	3.92	0.0049	4.47	1.89
2008	3.60	0.0020	5.49	2.12
2009	4.86	0.0012	3.21	1.27
2010	6.06	0.0029	4.32	1.21
2011	3.70	0.0025	2.68	0.62
2012	5.63	0.0015	4.01	0.66

Due to the opportunistic acquisition strategy of VHR satellites we were unable to obtain temporal stacks of VHR imagery, thus we were consequently unable to utilize pairs of VHR images in a pre- and post-burn validation assessment. Additionally, the VHR samples were not randomly selected (see Section 2.1.3 for further details). The accuracy assessment should therefore be viewed with these limitations in mind.

3.2. CRAB analysis

The total Russian cropland area as defined by the crop mask totals approximately 215×10^4 km^2. Using the full range of confidence values, our estimated annual burned area from CRAB within the Russian cropland ranged from approximately 121×10^4 km^2 (2007) to approximately 144×10^4 km^2 (2010), which equates to roughly 57–67% of the total cropland area. Applying a mapping confidence value of >60% on the spring output and using the full range of confidence values on the summer output, the annual burned area estimate decreased to between approximately 3.54×10^4 km^2 (2003) and 7.92×10^4 km^2 (2010), which equates to roughly 1–4% of the total Russian cropland area. The majority of the burned area occurred in spring (defined 1 March–30 June) as compared to summer (defined 1 July–30 September). Table 5 and Table 6 summarize the seasonal burned area estimates for CRAB (full confidence and >60% confidence values), MCD45A1 and MCD64A1 (see Section 2.3 for intercomparison between the three BA products).

Subdividing Russia into administrative units (oblasts) and Federal Districts (okrugs) revealed further information on the spatial and temporal patterns of burning. Analysis on the average fractional burned area per oblast between 2003 and 2012 (Table S2) revealed the general patterns of burned area produced by CRAB correspond with the known winter wheat and spring wheat oblasts. Additionally temporal analysis of the average fractional burned area between 2003 and 2012 revealed information about the relative contribution of spring and summer burning between the various okrugs (Fig. 10, Table S3). CRAB reported larger contributions of spring burning in the eastern okrugs whereas the southern and western okrugs contained a higher contribution of burning in the summer and early fall. This pattern is consistent with the winter and spring wheat agricultural practices in the region.

3.3. Intercomparison between CRAB, MCD45A1, and MCD64A1

When comparing the magnitude of mapped burned area for each of the three burned area products within the Russian cropland region it is clear that MCD64A1 and CRAB follow similar patterns of burned area frequency in the spring, while MCD45A1 contains considerable spikes (Fig. 11). Whereas in the summer, MCD45A1 and CRAB show considerable spikes throughout the season with MCD64A1 fairly muted in comparison (Fig. 12). The similarity in mapped burned area between MCD45A1 and CRAB may be related to external factors such as missed clouds or BRDF effects. For illustration purposes one example is shown

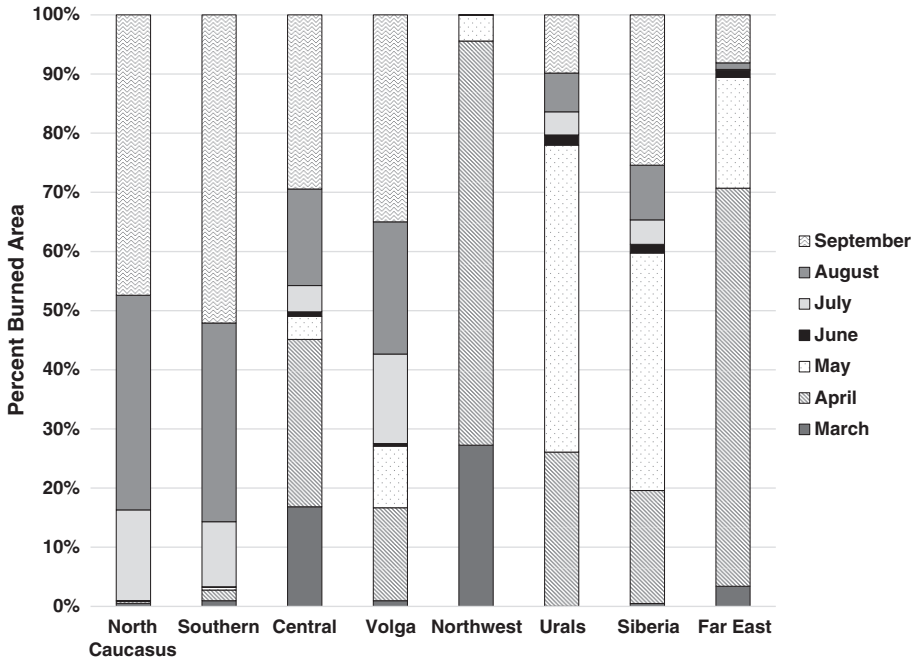

Fig. 10. Temporal distribution of the average fractional burned area by month between 2003 and 2012 for the Russian cropland region partitioned by Federal Districts (okrugs).

for each season but the relative patterns are consistent over all years (2003–2012).

When comparing the three burned area products' seasonal totals (Fig. 13), MCD45A1 generally has the higher magnitude of burning in the summer; however, there are a few years where CRAB and MCD45A1 have very similar magnitudes. Interestingly CRAB, and to some extent MCD45A1, saw a large spike of burned area in summer 2010 which was the season of extreme drought in Russia where widespread fires in forests and cropland in European Russia were reported.

Although based on different mapping algorithms, the similarities in the general burned area patterns between the three BA products reveals that using MODIS to map cropland burned area in Russia is not the solution as all three products contain large omission errors (Table 4) thus are not representing the true burned area within Russian croplands well.

4. Challenges of mapping

Successfully developing an accurate estimate of cropland burning in Russia is a difficult task due to the inherent challenges in meeting the particular mapping requirements. Cropland fires are transient in nature in comparison to grassland or forest fires. The short duration of the cropland burn scars, matched with the subsequent plowing of the fields, makes it difficult to capture the entirety of the cropland burned area

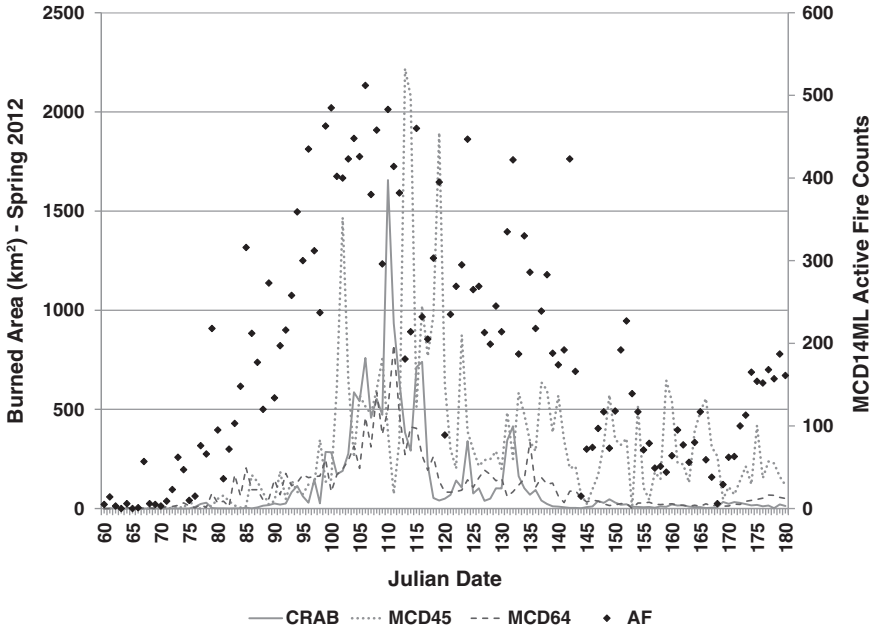

Fig. 11. Daily burned area (km^2) left axis and MODIS Active Fire counts right axis during spring 2012 for all Russian cropland MODIS tiles. All confidence values >60% were included for the CRAB product.

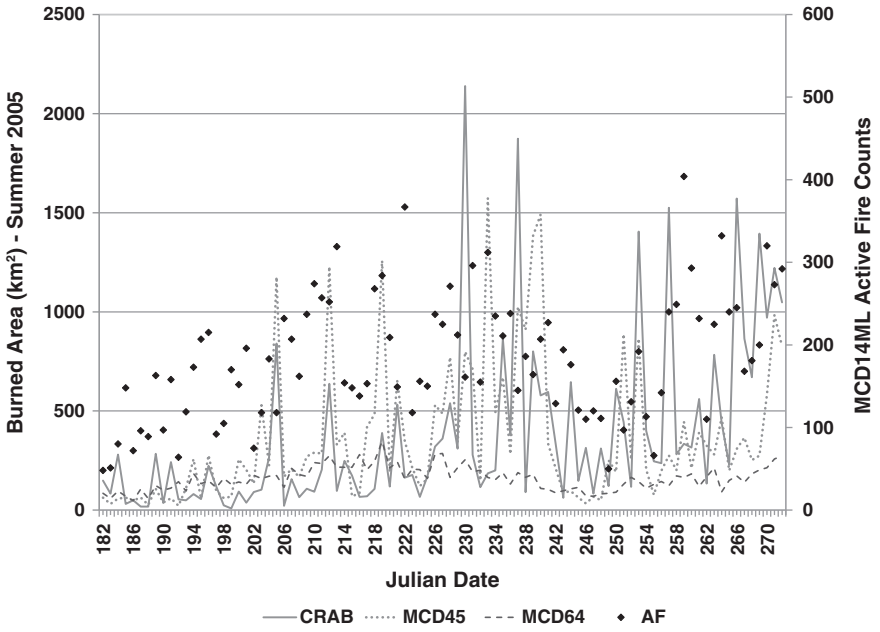

Fig. 12. Daily burned area (km^2) left axis and MODIS Active Fire counts right axis during summer 2005 for all Russian cropland MODIS tiles. All confidence values were included for the CRAB product.

without daily clear observations of moderate (10–50 m) spatial resolution over agricultural areas. Analysis carried out on the Russian cropland region between 2003 and 2012 (see Section 2.1 for additional details) shows that on average early afternoon observations from Aqua provided 51 clear views per growing period (defined as 1 March–30 September) with a range from 6 to 113 clear views; whereas Terra provided 61 clear views per growing period with a range from 14 to 114 clear views. Upon combination of the Aqua and Terra clear view time series, the analysis found an increase in the number of clear views with an average of 106 clear views per growing period with a range from 24 to 199 clear views (Fig. 14).

The best conditions were found in the eastern section of Rostovskaya Oblast, while the worst conditions were found along the southern tip of the Russian cropland near the Ingushetia Republic. Although there was an increase in the number of clear views using the combined Aqua and Terra clear surface view time series, the frontal systems that move across Russia lead to periods of several days to weeks with no clear view of the surface. This inability to view the surface for several consecutive days likely leads to underestimation in cropland burned area.

Although MODIS has a daily overpass, this high temporal frequency is countered by a coarse (≥500 m) spatial resolution. As previously

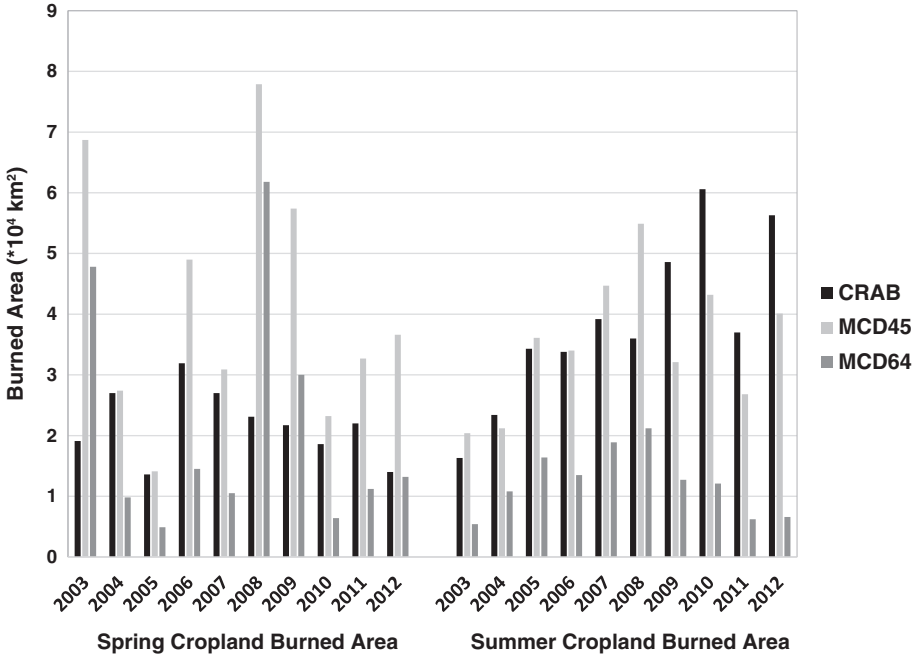

Fig. 13. Spring and summer cropland burned area (units: × 10^4 km^2 = Mha) comparison between CRAB (all confidence in fall and >60% confidence in spring), MCD45A1 and MCD64A1.

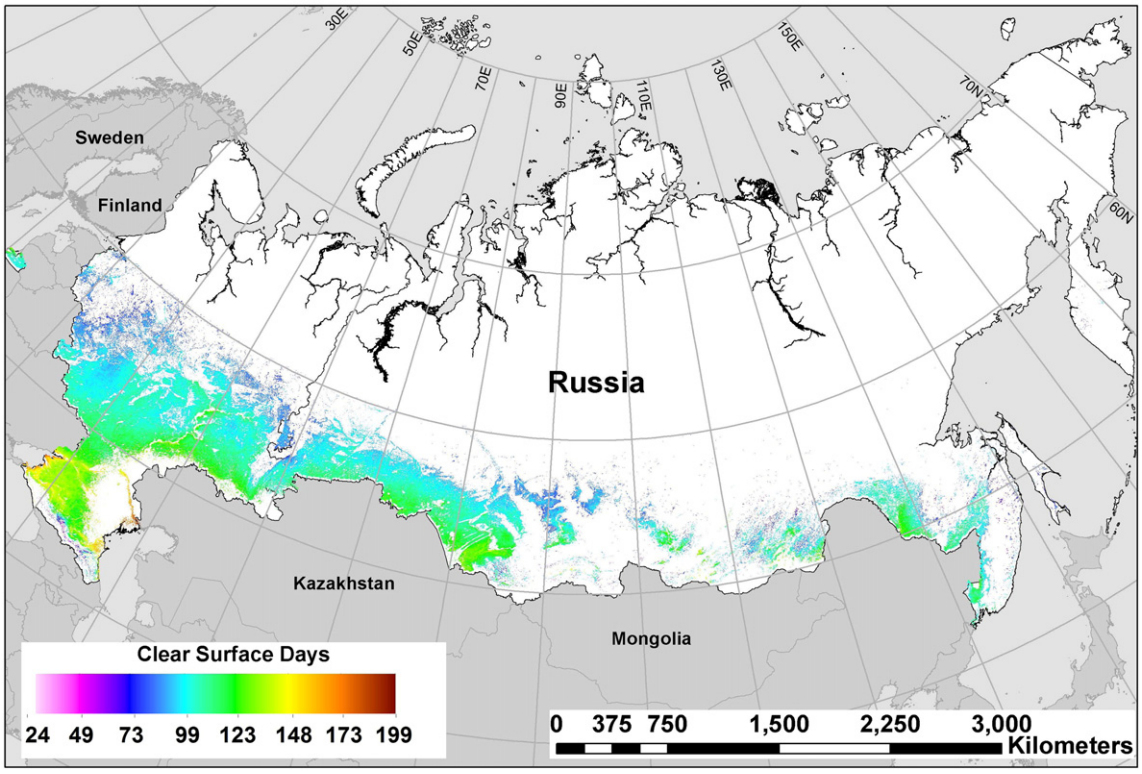

Fig. 14. Mean number of cropland clear surface days per year between 1 March and 30 September (2003 and 2012) as defined by the 1 km MODIS quality assessment bit thresholds as set out in Section 2.1. This image corresponds to the combined Aqua and Terra dataset for the Russian cropland region.

shown (Fig. 5, Table 1) the median size of observed burns is 40 ha (<2 MODIS 500 m grid cells) with a substantial amount of partial burning within the observed samples, therefore when using the MODIS 500 m daily surface reflectance data, the burned pixel's spectral signature is reduced in comparison with the surrounding unburned pixels. This decrease in spectral signature separability between field state types (burn, residue, plow and bare) further amplifies the difficulty in distinguishing between burned and plowed fields. This is a particular problem in the Mollisol soil regions, where the soil is characterized by its mollic epipedon which gives it a distinctive dark, almost black, appearance (Grunwald, 2015). As compared to other soil orders in the 350–2500 nm spectral range, Mollisol soils have the lowest reflectance curves with reflectance values <0.1 due to the high organic matter content (Sahoo, 2013). The low spectral reflectance throughout the visible, Near Infrared (NIR) and Shortwave Infrared (SWIR) portions of the electromagnetic spectrum can lead to further challenges in distinguishing Mollisol soils from older burn scars thereby leading to an increase in commission error and overestimation of burned area.

Spectral analysis was carried out on the VHR samples located in the dark soil (Mollisol, Vertisol and Chernozem; 92% of total VHR samples) regions and the light soil (Alfisol; 8% of total VHR samples) regions of the Russian cropland area both separately and combined. The dark soil samples showed no spectral separability between the burn and unburned categories with almost complete overlap between all four categories in all bands and spectral indices set out in Section 2.3, while the light soil samples showed some separability between the classes. Since the Russian cropland region contains predominately dark soils, we based the algorithm on all the samples regardless of soil type.

In addition to the low spectral contrast, the signal is further diluted due to the resampling error associated with aligning the irregularly shaped VHR samples with the coarse spatial resolution MODIS sinusoidal grid. The irregular shape of the fields and burn samples resulted in many of the matched pixels incorporating spectral signatures from surrounding areas. Analysis on the samples found that on average approximately 40% of the masked MODIS grid cells (Fig. 15, light grey squares)

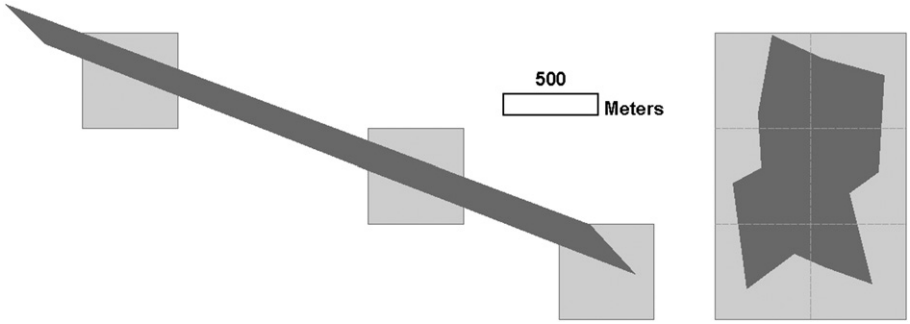

Fig. 15. MODIS grid cell area masks (light grey squares) and field boundary area (dark grey shapes) overlay analysis.

were outside of the field boundary (Fig. 15, dark grey shapes) and on average approximately 25% of the field boundaries were outside of the masked MODIS grid cells. Fig. 15 highlights two examples of the impact of the alignment of the VHR samples onto the MODIS 500 m sinusoidal grid and the introduction of mixed pixels into the sample's spectral signature.

Furthermore, at higher latitudes MODIS data are comprised of multi-angular observations compiled from the best available pixels acquired from as many as four overpasses to generate the daily image for Aqua and Terra (Schaaf et al., 2002; Loboda et al., 2011). Combining these multi-angular observations with the relative day-to-day variations in viewing and illumination geometries, in addition to the impacts of cloud cover and changing surface properties, leads to substantial BRDF effects. These effects produce radiometrically inconsistent views of the surface thereby further impacting the stability of the burn spectral signature.

5. Conclusion

Although agricultural burning is banned in Russia it is still a widespread practice (Pettus, 2009) and the challenges associated with mapping cropland burning have led to a wide range of burned area estimates. Accurate monitoring of cropland burning is an important task as countless studies have relied on these estimates for use in emission calculations for air quality and human health studies, in addition to studies on the impact of emissions on climate forcing (e.g. Jacobson, 2004; Lin et al., 2012; McCarty et al., 2012; Stohl et al., 2006; Witham and Manning, 2007).

In this study, we assessed three very different MODIS-based burned area algorithms which operate on the same input data and based on our analysis we concluded that coarse resolution (≥500 m) instruments, such as MODIS, are not optimal for mapping these small, short-lived fires. Our study demonstrates this through the analysis of the current MODIS-based products (MCD45A1 and MCD64A1) and our own custom MODIS-based burned area product. Clearly we did not complete an exhaustive analysis of all possible algorithms and although there are other algorithms we have no recommendations about what these should look like. In addition, we were also able to identify major deficiencies in the MODIS data related to mapping cropland burning which we addressed in Section 4.

Ultimately, the current coarse resolution (≥500 m) satellite capabilities are not adequate for measurement of burned area associated with agricultural fires. Coarse resolution (≥500 m) sensors like MODIS have the advantage of daily overpasses which are essential when mapping a transient process such as cropland residue burning; however, the small spatial scale of these burns requires moderate (10–50 m) spatial resolutions. The current moderate (10–50 m) resolution sensors like Landsat have the higher spatial resolutions; however, the 8–16 day repeat cycle (considering the possible constellation of two satellites as was achieved with Landsat 5 and 7 and is currently achieved with Landsat 7 and 8) is a limitation in mapping cropland burning. The preference to burn the remaining post-harvest residue as close to planting as possible leads to an increased likelihood of overlooking the burn signal without daily clear surface observations (Korontzi et al., 2006; Shoyer et al., 2013). Finally the very high resolution (<5 m pixel) sensors like QuickBird have the high resolution needed to identify field state (plowed, burned, growing crop, or harvested); however there is no systematic data acquisition strategy which ultimately leads to opportunistic observations that do not support time series analyses. Future opportunities to accurately map cropland burned area may arise with the Sentinel-2 and Landsat constellation missions.

Acknowledgments

This project was supported by the U.S. Department of Agriculture: Black Carbon Initiative funded by a grant from the U.S. Department of State (S-OES-10-IAA-0025) under the oversight of Mr. B Kinder (USDA Forest Service). The authors would like to thank the National Geospatial Intelligence Agency for providing us with the very high resolution imagery and the image analysts; K. Ageh, R. Crawford, A. Culp-Cano, A. Hoffman-Hall, P. McDonough and, L. Wang from the University of Maryland and S. Devereaux from the USDA ARS for assisting with data download and digitizing the VHR archive.

Appendix A. Supplementary data

Supplementary data to this article can be found online at http://dx.doi.org/10.1016/j.rse.2016.07.022.

References

Bond, T.C., Doherty, S.J., Fahey, D.W., Forster, P.M., Berntsen, T., DeAngelo, B.J., Flanner, M.G., Ghan, S., Karcher, B., Koch, D., Kinne, S., Kondo, Y., Quinn, P.K., Sarofim, M.C., Schultz, M.G., Schulz, M., Venkataraman, C., Zhang, H., Zhang, S., Bellouin, N., Guttikunda, S.K., Hopke, P.K., Jacobson, M.Z., Kaiser, J.W., Klimont, Z., Lohmann, U., Schwarz, J.P., Shindell, D., Storelvmo, T., Warren, S.G., Zender, C.S., 2013. Bounding the role of black carbon in the climate system: A scientific assessment. J. Geophys. Res.-Atmos. 118, 5380–5552. http://dx.doi.org/10.1002/jgrd.50171.

Carroll, M.L., Townshend, J.R., DiMiceli, C.M., Noojipady, P., Sohlberg, R.A., 2009. A new global raster water mask at 250 m resolution. Int. J. Digital Earth 2, 291–308. http://dx.doi.org/10.1080/17538940902951401.

Chuvieco, E., Opazo, S., Sione, W., Valle, H.D., Anaya, J., Bella, C.D., Cruz, I., Manzo, L., López, G., Mari, N., González-Alonso, F., 2008. Global burned-land estimation in Latin America using MODIS composite data. Ecol. Appl. 18 (1), 64–79.

EPA, US Environmental Protection Agency's Agricultural Center, 2012e. Agricultural Burning. http://www.epa.gov/agriculture/tburn.html (Last accessed 8/22/2015).

FAOSTAT, 2015a. http://faostat3.fao.org/browse/E/EL/E (Last accessed 8/22/2015).

FAOSTAT, 2015b. http://faostat3.fao.org/browse/T/TP/E (Last accessed 8/22/2015).

Foley, J.A., DeFries, R., Asner, G.P., Barford, C., Bonan, G., Carpenter, S.R., Chapin, F.S., Coe, M.T., Daily, G.C., Gibbs, H.K., Helkowski, J.H., Holloway, T., Howard, E.A., Kucharik, C.J., Monfreda, C., Patz, J.A., Prentice, I.C., Ramankutty, N., Snyder, P.K., 2005. Global consequences of land use. Science 309, 570–574. http://dx.doi.org/10.1126/science.1111772.

Friedl, M.A., Sulla-Menashe, D., Tan, B., Schneider, A., Ramankutty, N., Sibley, A., Huang, X., 2010. MODIS collection 5 global land cover: algorithm refinements and characterization of new datasets. Remote Sens. Environ. 114, 168–182.

Galvao, L.S., Roberts, D.A., Formaggio, A.R., Numata, I., Breunig, F.M., 2009. View angle effects on the discrimination of soybean varieties and on the relationships between vegetation indices and yield using off-nadir Hyperion data. Remote Sens. Environ. 113, 846–856. http://dx.doi.org/10.1016/j.rse.2008.12.010.

Gao, B.C., 1996. NDWI—a normalized difference water index for remote sensing of vegetation liquid water from space. Remote Sens. Environ. 58 (3), 257–266.

Giglio, L., Descloitres, J., Justice, C.O., Kaufman, Y.J., 2003. An enhanced contextual fire detection algorithm for MODIS. Remote Sens. Environ. 87, 273–282.

Giglio, L., Loboda, T., Roy, D.P., Quayle, B., Justice, C.O., 2009. An active-fire based burned area mapping algorithm for the MODIS sensor. Remote Sens. Environ. 113, 408–420. http://dx.doi.org/10.1016/j.rse.2008.10.006.

Grumm, R.H., 2011. The Central European and Russian heat event of Jul–August 2010. Bull. Am. Meteorol. Soc. 92, 1285–1296.

Grunwald, S., 2015. Mollisols. University of Florida, Soil and Water Science Departmenthttps://soils.ifas.ufl.edu/faculty/grunwald/teaching/eSoilScience/mollisols.shtml (Last accessed 8/22/2015).

Hansen, J., Nazarenko, L., 2004. Soot Climate Forcing via Snow and Ice Albedos. Proceedings of the National Academy of Sciences of the United States of America. 101, pp. 423–428. http://dx.doi.org/10.1073/pnas.2237157100.

Hegg, D.A., Warren, S.G., Grenfell, T.C., Doherty, S.J., Larson, T.V., Clarke, A.D., 2009. Source attribution of black carbon in Arctic snow. Environ. Sci. Technol. 43, 4016–4021. http://dx.doi.org/10.1021/es803623f.

Jacobson, M.Z., 2004. The short-term cooling but long-term global warming due to biomass burning. J. Clim. 17, 2909–2926. http://dx.doi.org/10.1175/1520-0442(2004)017<2909:TSCBLG>2.0.CO;2.

Jacobson, M.Z., Bond, T.C., Ramanathan, V., Zender, C., Schwartz, J., 2007. Hearing examines black carbon and global warming. House Committee on Oversight and Government Reform Testimony. http://tinyurl.com/yz2jesv (Last accessed 8/22/2015)

Kramer, A.E., 2010. Drought in Russia Ripples Beyond the Wheat Fields. The New York Times: Global Business (Last accessed 08/26/2015).

Koch, D., Hansen, J., 2005. Distant origins of Arctic black carbon: A Goddard Institute for Space Studies ModelE experiment. J. Geophys. Res.-Atmos. 110. http://dx.doi.org/10.1029/2004jd005296.

Korontzi, S., McCarty, J., Loboda, T., Kumar, S., Justice, C., 2006. Global distribution of agricultural fires in croplands from 3 years of moderate resolution imaging spectroradiometer (MODIS) data. Glob. Biogeochem. Cycles 20, GB2021. http://dx.doi.org/10.1029/2005GB002529.

Korontzi, S., McCarty, J., Justice, C., 2008. Monitoring agricultural burning in the mississippi River Valley Region from the moderate resolution imaging spectroradiometer (MODIS). J. Air Waste Manage. Assoc. 58 (9), 1235–1239.

Law, K.S., Stohl, A., 2007. Arctic air pollution: Origins and impacts. Science 315, 1537–1540. http://dx.doi.org/10.1126/science.1137695.

Lin, H.W., Jin, Y.F., Giglio, L., Foley, J.A., Randerson, J.T., 2012. Evaluating greenhouse gas emissions inventories for agricultural burning using satellite observations of active fires. Ecol. Appl. 22, 1345–1364.
Loboda, T., O'Neal, K.J., Csiszar, I., 2007. Regionally adaptable dNBR-based algorithm for burned area mapping from MODIS data. Remote Sens. Environ. 109, 429–442.
Loboda, T.V., Hoy, E.E., Giglio, L., Kasischke, E.S., 2011. Mapping burned area in Alaska using MODIS data: a data limitations-driven modification to the regional burned area algorithm. Int. J. Wildland Fire 20, 487–496. http://dx.doi.org/10.1071/wf10017.
Lopez, M.J., Caselles, V., 1991. Mapping burns and natural reforestation using thermatic mapper data. Geocarto Int. 6 (1), 31–37.
McCarty, J.L., Ellicott, E.A., Romanenkov, V., Rukhovitch, D., Koroleva, P., 2012. Multi-year black carbon emissions from cropland burning in the Russian Federation. Atmos. Environ. 63, 223–238. http://dx.doi.org/10.1016/j.atmosenv.2012.08.053.
McCarty, J.L., Korontzi, S., Justice, C.O., Loboda, T., 2009. The spatial and temporal distribution of crop residue burning in the contiguous United States. Sci. Total Environ. 407, 5701–5712. http://dx.doi.org/10.1016/j.scitotenv.2009.07.009.
McCarty, J.L., Loboda, T., Trigg, S., 2008. A hybrid remote sensing approach to quantifying crop residue burning in the United States. Appl. Eng. Agric. 24, 515–527.
Pettus, A. (2009). Agricultural Fires and Arctic Climate Change: A Special CATF Report. In pp. 1–33: Clean Air Task Force.
Quinn, P.K., Bates, T.S., Baum, E., Doubleday, N., Fiore, A.M., Flanner, M., Fridlind, A., Garrett, T.J., Koch, D., Menon, S., Shindell, D., Stohl, A., Warren, S.G., 2008. Short-lived pollutants in the Arctic: their climate impact and possible mitigation strategies. Atmos. Chem. Phys. 8, 1723–1735. http://dx.doi.org/10.5194/acp-8-1723-2008.
Quinn, P.K., Stohl, A., Arneth, A., Berntsen, T., Burkhart, J.F., Christensen, J., Flanner, M., Kupiainen, K., Lihavainen, H., Shepherd, M., Shevchenko, V., Skov, H., Vestreng, V., 2011. The Impact of Black Carbon on Arctic Climate. AMAP Technical Report No. 4. Arctic Monitoring and Assessment Programme (AMAP), Oslo.
Rahman, H., Quadir, D., Zahedul Islam, A., Dutta, S., 1999. Viewing angle effect on the remote sensing monitoring of wheat and rice crops. Geocarto Int., (Hong Kong), pp. 74–79.
Ramanathan, V., Carmichael, G., 2008. Global and regional climate changes due to black carbon. Nat. Geosci. 1, 221–227. http://dx.doi.org/10.1038/ngeo156.
Ramankutty, N., Evan, A.T., Monfreda, C., Foley, J.A., 2008. Farming the planet: 1. Geographic distribution of global agricultural lands in the year 2000. Glob. Biogeochem. Cycles 22.
Randerson, J.T., Chen, Y., van derWerf, G.R., Rogers, B.M., Morton, D.C., 2012. Global burned area and biomass burning emissions from small fires. J. Geophys. Res. 117, G04012. http://dx.doi.org/10.1029/2012JG002128.
Ranson, K.J., Daughtry, C.S.T., Biehl, L.L., Bauer, M.E., 1985. Sun-view angle effects on reflectance factors of corn canopies. Remote Sens. Environ. 18, 147–161. http://dx.doi.org/10.1016/0034-4257(85)90045-8.
Rouse Jr., J., Haas, R.H., Schell, J.A., Deering, D.W., 1974. Monitoring vegetation systems in the Great Plains with ERTS. NASA Spec. Publ. 351, 309.
Roy, D., Jin, Y., Lewis, P., Justice, C., 2005. Prototyping a global algorithm for systematic fire-affected area mapping using MODIS time series data. Remote Sens. Environ. 97, 137–162.
Roy, D.P., Boschetti, L., Justice, C.O., Ju, J., 2008. The collection 5 MODIS burned area product - global evaluation by comparison with the MODIS active fire product. Remote Sens. Environ. 112, 3690–3707. http://dx.doi.org/10.1016/j.rse.2008.05.013.
Sahoo, R., 2013. Hyperspectral Remote Sensing. Indian Agricultural Statistics Research Institute, New Delhi 110 012. http://www.iasri.res.in/ebook/GIS_TA/M2_4_HYSRS.pdf (Last accessed 10/01/2015).
Schaaf, C.B., Gao, F., Strahler, A.H., Lucht, W., Li, X.W., Tsang, T., Strugnell, N.C., Zhang, X.Y., Jin, Y.F., Muller, J.P., Lewis, P., Barnsley, M., Hobson, P., Disney, M., Roberts, G., Dunderdale, M., Doll, C., d'Entremont, R.P., Hu, B.X., Liang, S.L., Privette, J.L., Roy, D., 2002. First operational BRDF, albedo nadir reflectance products from MODIS. Remote Sens. Environ. 83, 135–148. http://dx.doi.org/10.1016/S0034-4257(02)00091-3.
Shindell, D.T., Chin, M., Dentener, F., Doherty, R.M., Faluvegi, G., Fiore, A.M., Hess, P., Koch, D.M., MacKenzie, I.A., Sanderson, M.G., Schultz, M.G., 2008. A multi-model assessment of pollution transport to the Arctic. Atmos. Chem. Phys. 8 (17), 5353–5372.
Shoyer, J., Peterson, D., Presely, D., DeWolf, E., Whitworth, J., 2013. Pros and cons of burning wheat residue before planting. Kansas State University. http://www.agprofessional.com/resource-centers/wheat/disease/news/Pros-and-cons-of-burning-wheat-residue-before-planting-226956471.html (Last accessed 09/30/2015).
Sovecon. (2013). Agricultural Burning Survey Report Prepared for US Forest Service. Personal communication with Dr. Wei Min Hao – Missoula Fire Lab.
Stohl, A., 2006. Characteristics of atmospheric transport into the Arctic troposphere. J. Geophys. Res.-Atmos. 111.
Stohl, A., Andrews, E., Burkhart, J.F., Forster, C., Herber, A., Hoch, S.W., Kowal, D., Lunder, C., Mefford, T., Ogren, J.A., Sharma, S., Spichtinger, N., Stebel, K., Stone, R., Strom, J., Torseth, K., Wehrli, C., Yttri, K.E., 2006. Pan-Arctic enhancements of light absorbing aerosol concentrations due to North American boreal forest fires during summer 2004. J. Geophys. Res.-Atmos. 111. http://dx.doi.org/10.1029/2006jd007216.
Stohl, A., Berg, T., Burkhart, J.F., Fjaeraa, A.M., Forster, C., Herber, A., Hov, O., Lunder, C., McMillan, W.W., Oltmans, S., Shiobara, M., Simpson, D., Solberg, S., Stebel, K., Strom, J., Torseth, K., Treffeisen, R., Virkkunen, K., Yttri, K.E., 2007. Arctic smoke - record high air pollution levels in the European Arctic due to agricultural fires in Eastern Europe in spring 2006. Atmos. Chem. Phys. 7, 511–534.
Stocker, T.F., Qin, D., Plattner, G.K., Alexander, L.V., Allen, S.K., Bindoff, N.L., Bréon, F.M., Church, J.A., Cubash, U., Emori, S., Forster, P., Friedlingstein, P., Gillett, N., Gregory, J.M., Hartmann, D.L., Jansen, E., Kirtman, B., Knutti, R., Krishna Kumar, K., Lemke, P., Marotzke, J., Masson-Delmotte, V., Meehl, G.A., Mokhov, I.I., Piao, S., Ramaswamy, V., Randall, D., Rhein, M., Rojas, M., Sabine, C., Shindell, D., Talley, L.D., Vaughan, D.G., Xie, S.P., 2013. Technical Summary: The Physical Science Basis. Contribution of Working Group I to the Fifth Assessment Report of the Intergovernmental Panel on Climate Change. Cambridge University Press, Cambridge, United Kingdom and New York, NY, USA.
Trigg, S., Flasse, S., 2000. Characterizing the spectral-temporal response of burned savannah using in situ spectroradiometry and infrared thermometry. Int. J. Remote Sens. 21 (16), 3161–3168.
USDA FAS (Foreign Agricultural Service), 2013. Russia: Agricultural Overview. Production Estimates and Crop Assessment Division. http://www.fas.usda.gov/pecad2/highlights/2005/03/Russia_Ag/ (Last accessed 02/06/2014).
Vermote, E.F., Kotchenova, S.Y., Ray, J.P., 2011. MODIS Surface Reflectance (MOD/MYD09) User's Guide. Version 1.3. http://modis-sr.ltdri.org/guide/MOD09_UserGuide_v1_3.pdf (Last accessed 8/26/2015).
Warneke, C., Froyd, K.D., Brioude, J., Bahreini, R., Brock, C.A., Cozic, J., de Gouw, J.A., Fahey, D.W., Ferrare, R., Holloway, J.S., Middlebrook, A.M., Miller, L., Montzka, S., Schwarz, J.P., Sodemann, H., Spackman, J.R., Stohl, A., 2010. An important contribution to springtime Arctic aerosol from biomass burning in Russia. Geophys. Res. Lett. 37, L01801. http://dx.doi.org/10.1029/2009gl041816.
Witham, C., Manning, A., 2007. Impacts of Russian biomass burning on UK air quality. Atmos. Environ. 41, 8075–8090. http://dx.doi.org/10.1016/j.atinosenv.2007.06.058.
Wu, M., Knorr, W., Thonicke, K., Schurgers, G., Camia, A., Arneth, A., 2015. Sensitivity of burned area in Europe to climate change, atmospheric CO_2 levels, and demography: a comparison of two fire-vegetation models. J. Geophys. Res. Biogeosci. 120, 2256–2272. http://dx.doi.org/10.1002/2015JG003036.
Zender, C.S., 2007. Arctic Climate Effects of Black Carbon. http://dust.ess.uci.edu/ppr/ppr_hogrc_wrt.pdf (Last accessed 02/27/2016).
Zhang, Y.H., Wooster, M.J., Tutubalina, O., Perry, G.L.W., 2003. Monthly burned area and forest fire carbon emission estimates for the Russian Federation from SPOT VGT. Remote Sens. Environ. 87, 1–15. http://dx.doi.org/10.1016/s0034-4257(03)00141-x.